Coastal Engineering in Japan, Vol. 39, No. 2, 1996

NUMERICAL GENERATION AND PROPAGATION OF PERIODICAL WAVES IN TIME DOMAIN

Chung-Ren Chou [1]
Ruey-Syan Shih [2]

ABSTRACT

Generation of two dimensional nonlinear waves is simulated numerically by boundary element method. The present scheme is based on the Lagrangian description together with finite difference to the time step. An algorithm to generate waves with any prescribed form is also implanted in the method. The numerical model is verified by studying the case of periodical waves impinging against a vertical wall. Time histories of the evolution of two dimensional periodical waves running up on a sloping beach as well as the distribution of current velocity within the fluid region are then presented.

Keywords: nonlinear waves, boundary element method, Lagrangian description, wave-making

I. INTRODUCTION

Problems associated with wave generation, propagation and deformation have been studied numerically by many researchers. Based on the linearized governing equations, Madsen (1970) used a mathematical model for the particular problem of the wave generated by a sinusoidally moving piston-type wavemaker. Faltinsen (1978) presented a numerical method for studying the sloshing in a wave tank with a two-dimensional flow. According to Green's formula, Nakayama (1983) applied a new boundary element technique to the analysis of nonlinear water wave problems, including two wave-making problems. Brorsen and Larsen (1987) reported a new approach to the generation of waves in a boundary integral equation model for nonlinear regular waves. With the well-known Green's theorem, a time-domain second-order method for the simulation of transient, nonlinear wave propagation in a flume was then developed by Isaacson *et al.* (1994). Besides, by the finite element method, a two-dimensional nonlinear time domain free surface flow problem was analyzed by Wu and Taylor (1995), and the numerical results were given for the vertical wave maker problem and for a transient wave in a rectangular container. Chou *et al.* (1996) studied the deformation of nonlinear waves in coastal zones with submerged obstacle by using the boundary element method.

In this study, two-dimensional nonlinear wave-making problems are considered numerically by boundary element method. The algorithm is based on the Largrangian

[1]Dr. Eng., Professor, Dept. of Harbor and River Eng., National Taiwan Ocean University, Taiwan.
[2]M.E., Doctoral Student, ditto.

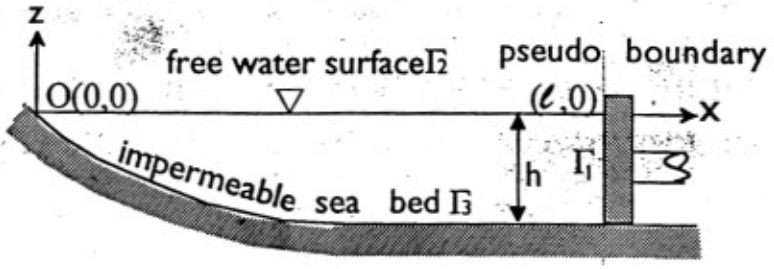

Fig. 1 Defintion sketch.

description and finite difference of the time domain. In the present numerical model, a scheme to generate waves with any prescribed form is implanted. The stability of the model will be cross-checked by the constancy of mass and energies.

II. THEORETICAL FORMULATION

As shown in Fig. 1, a Cartesian coordinate system is employed. The origin is located on the still water level and the z-axis is positively upwards. The flow field is bounded by the pseudo wave-generating boundary Γ_1, the free water surface Γ_2 and the impermeable sea bed Γ_3. Assuming that the pseudo wave-generating boundary Γ_1 is sufficiently far away from the coastal zone, wave scattering induced by undersea topography or obstacles can be neglected. The fluid within the region is assumed to be inviscid and incompressible, and the flow to be irrotational. Fluid motion then has a velocity potential $\Phi(x, z; t)$ satisfying the following Laplace equation:

$$\frac{\partial^2 \Phi}{\partial x^2} + \frac{\partial^2 \Phi}{\partial z^2} = 0 \tag{1}$$

2.1 Boundary Conditions

(1) Boundary Condition on Pseudo Wave-Making Boundary

The boundary Γ_1 is assumed to represent a wave-generating device. In this study, a piston wave generator is assumed for simplicity, although it is clear that paddle of any desired type can be simulated. Requiring that the horizontal velocities of the pseudo wave-paddle $U(t)$ and the adjacent fluid flow be continuous, we obtain the following relationship:

$$\overline{\Phi} = \frac{\partial \Phi}{\partial \nu} = U(t) \tag{2}$$

where ν is the unit normal.

Wave with prescribed form can be simulated by selecting suitable input $U(t)$. In this study, periodical waves are simulated. $U(t)$ can then be expressed as

$$U(t) = -a\sigma \sin \sigma t \tag{3}$$

$$a = \zeta_0 \frac{\sinh kh \cosh kh + kh}{2 \sinh^2 kh} \tag{4}$$

Where σ ($=2\pi/T$) is the angular frequency, ζ_0 is the wave amplitude, k is the wave number, h is the constant water depth, and T is the period of the wave to be generated.

(2) Boundary Condition on Free Water Surface

The atmospheric pressure is assumed to be constant. Boundary conditions on the free water surface can thus be obtained from the kinematic and dynamic conditions as follows:

$$u = \frac{Dx}{Dt} = \frac{\partial \Phi}{\partial x} \tag{5}$$

$$w = \frac{Dz}{Dt} = \frac{\partial \Phi}{\partial z} \tag{6}$$

$$\frac{D\Phi}{Dt} + g\zeta - \frac{1}{2}\left[\left(\frac{\partial \Phi}{\partial x}\right)^2 + \left(\frac{\partial \Phi}{\partial z}\right)^2\right] = 0 \tag{7}$$

where D is the Lagrange differentiation, g is the gravitational acceleration, and ζ is the surface elevation.

(3) Boundary Condition on Sea Bed

The water particle velocity is null in the normal direction on the impermeable seabed:

$$\frac{\partial \Phi}{\partial \nu} = 0 \tag{8}$$

2.2 The Integral Equations

According to Green's second identity, velocity potential $\Phi(x, z; t)$ at any point within the region can be expressed by the velocity potential and its normal derivative on the boundary as

$$\Phi(x, z; t) = \frac{1}{2\pi}\int_\Gamma \left[\frac{\partial \Phi(\xi, \eta; t)}{\partial \nu} \ln\frac{1}{r} - \Phi(\xi, \eta; t)\frac{\partial}{\partial \nu}\ln\frac{1}{r}\right] ds \tag{9}$$

where $r = [(\xi - x)^2 + (\eta - z)^2]^{\frac{1}{2}}$.

When the inner point (x, z) approaches the boundary point (ξ', η'), due to its singularity, the velocity potential $\Phi(\xi, \eta; t)$ can be expressed as:

$$\Phi(\xi', \eta'; t) = \frac{1}{\pi}\int_\Gamma \left[\frac{\partial \Phi(\xi, \eta; t)}{\partial \nu} \ln\frac{1}{R} - \Phi(\xi, \eta; t)\frac{\partial}{\partial \nu}\ln\frac{1}{R}\right] ds \tag{10}$$

where $R = [(\xi - \xi')^2 + (\eta - \eta')^2]^{\frac{1}{2}}$.

In order to proceed with the numerical calculation, the boundaries Γ_1 through Γ_3 are divided into N_1 to N_3 discrete segments with linear elements, the above equation can then be written in a discretized form as

$$\Phi_i(\xi', \eta', t) + \frac{1}{\pi}\sum_{j=1}^{N}\int_{\Gamma_j} [\Phi_j(\xi, \eta, t)M_1 + \Phi_{j+1}(\xi, \eta, t)M_2]\frac{\partial}{\partial \nu}\ln\frac{1}{r} ds$$

$$= \frac{1}{\pi}\sum_{j=1}^{N}\int_{\Gamma_j} [\overline{\Phi}_j(\xi, \eta, t)M_1 + \overline{\Phi}_{j+1}(\xi, \eta, t)M_2]\ln\frac{1}{r} ds \tag{11}$$

where $N = N_1 + N_2 + N_3$, $\overline{\Phi}_j = \partial\Phi_j/\partial\nu$, $\overline{\Phi}_{j+1} = \partial\Phi_{j+1}/\partial\nu$, and M_1, M_2 are the shape functions; $M_1 = (1-\chi)/2$, $M_2 = (1+\chi)/2$, and χ is a local dimensionless coordinate.

Equation (11) can be expressed in a matrix form as

$$[\Phi] = [O]\,[\overline{\Phi}] \tag{12}$$

where $[\Phi]$ and $[\overline{\Phi}]$ are, respectively, formed by the nodal values of the potential function and its normal derivative on the boundaries, and $[O]$ is a matrix related to the geometrical shape of the boundary;

$$\left.\begin{aligned}
[\Phi] &= \Phi_i, \quad (i = 1 \sim N)\\
[\overline{\Phi}] &= \overline{\Phi}_i = \partial\Phi_i/\partial\nu \quad (i = 1 \sim N)\\
[O] &= [H + I]^{-1}\,[G]\\
[H] &= H_{ij}, \quad (i,j = 1 \sim N)\\
[G] &= G_{ij}, \quad (i,j = 1 \sim N)\\
H_{ij} &= \begin{cases} \overline{H}_{ij} & (i \neq j)\\ \overline{H}_{ij} + 1 & (i = j) \end{cases}\\
[I] &= \text{unit matrix}\\
\overline{H}_{ij} &= \begin{cases} h^1_{ij} + h^2_{ij-1} & (j \geq 2)\\ h^1_{i1} + h^2_{iN} & (j = 1) \end{cases}\\
G_{ij} &= \begin{cases} g^1_{ij} + g^2_{ij-1} & (j \geq 2)\\ g^1_{i1} + g^2_{iN} & (j = 1) \end{cases}
\end{aligned}\right\} \tag{13}$$

$$h^1_{ij} = \frac{1}{\pi}\int_{\Gamma_j} M_1 \frac{\partial}{\partial\nu}\ln\frac{1}{r}\,d\Gamma \tag{14}$$

$$h^2_{ij} = \frac{1}{\pi}\int_{\Gamma_j} M_2 \frac{\partial}{\partial\nu}\ln\frac{1}{r}\,d\Gamma \tag{15}$$

$$g^1_{ij} = \frac{1}{\pi}\int_{\Gamma_j} M_1 \ln\frac{1}{r}\,d\Gamma \tag{16}$$

$$g^2_{ij} = \frac{1}{\pi}\int_{\Gamma_j} M_2 \ln\frac{1}{r}\,d\Gamma \tag{17}$$

The numerical scheme has been discussed in detail by Chou (1983).

To facilitate the procedure of substituting the boundary conditions into each boundary, we rewrite Eq. (12) as the assembling of the following relations:

$$[\Phi_i] = [O_{ij}]\,[\overline{\Phi}_j], \quad i,j = 1 \sim 3 \tag{18}$$

2.3 A System of Equations

(1) The initial conditions on each boundary are summarized as follows

1) The pseudo wave-generating boundary Γ_1

Requirement of continuity between horizontal velocity of the pseudo wave-paddle $U(t)$ and the fluid motion gives rise to

$$\overline{\Phi}_1^0 = \frac{\partial \Phi_1^0}{\partial \nu} = -U(0) \tag{19}$$

where superscript 0 denotes the beginning time of the simulation.

2) The free water surface Γ_2

Assuming that the water surface is initially at rest ($t = 0$), the velocity potential is therefore null, *i.e.*,

$$\Phi_2^0 = 0 \tag{20}$$

3) The impermeable sea bed Γ_3

The flow is null in the direction normal to the impermeable seabed. Therefore,

$$\overline{\Phi}_3^0 = \frac{\partial \Phi_3^0}{\partial \nu} = 0 \tag{21}$$

(2) The finite difference of related terms

The tangential derivative on the free water surface, $(\partial \Phi_2/\partial s)_i$, can be approximated through

$$\left.\begin{aligned}
\left(\frac{\partial \Phi_2}{\partial s}\right)_i &= \left(\frac{\Delta s_i}{\Delta s_{i+1}}\right) \cdot \Phi_{2,i+1}/s' + (\Delta s_{i+1} - \Delta s_i) \cdot \Phi_{2,i}/s'' \\
&\quad - \left(\frac{\Delta s_{i+1}}{\Delta s_i}\right) \cdot \Phi_{2,i-1}/s' \\
\Delta s_i &= \sqrt{(x_{i+1} - x_i)^2 + (z_{i+1} - z_i)^2} \\
s' &= \Delta s_{i+1} + \Delta s_i \quad , \quad s'' = \Delta s_i \cdot \Delta s_{i+1}
\end{aligned}\right\} \tag{22}$$

where s denotes the tangential direction of the free water surface. On the free surface, we have

$$\left.\begin{aligned}
\frac{\partial \Phi_2}{\partial x} &= \frac{\partial \Phi_2}{\partial \nu} \sin\beta - \frac{\partial \Phi_2}{\partial s} \cos\beta \\
\frac{\partial \Phi_2}{\partial z} &= \frac{\partial \Phi_2}{\partial \nu} \cos\beta + \frac{\partial \Phi_2}{\partial s} \sin\beta
\end{aligned}\right\} \tag{23}$$

where β is the angle between the free water surface and the x-axis.

At the k-th time step, the profile of free water surface is expressed by (x^k, z^k). From Eqs. (5) and (6) we can evaluate that at the $(k+1)$-th time step which is expressed by (x^{k+1}, z^{k+1}) as follows:

$$x^{k+1} = x^k + \left(\frac{\partial \Phi_2^k}{\partial x}\right) \Delta t \tag{24}$$

$$z^{k+1} = z^k + \left(\frac{\partial \Phi_2^k}{\partial z}\right)\Delta t \tag{25}$$

where Δt denotes the discreted time difference interval.

From Eqs. (7) and (23), the velocity potential of the free water surface at the (k+1)-th time step, Φ^{k+1}, can be approximated through

$$\Phi_2^{k+1} = \Phi_2^k + \frac{1}{2}\left[\left(\frac{\partial \Phi_2}{\partial s}\right)^2 + \left(\frac{\partial \Phi_2}{\partial \nu}\right)^2\right]^k \Delta t - g z^{k+1}\Delta t \tag{26}$$

Substituting Eqs. (2), (8) and (26) into Eq. (18), we can obtain the following simultaneous equations.

$$\begin{bmatrix} \Phi_1 \\ \overline{\Phi}_2 \\ \Phi_3 \end{bmatrix}^{k+1} = \begin{bmatrix} I & -O_{12} & 0 \\ 0 & -O_{22} & 0 \\ 0 & -O_{32} & I \end{bmatrix}^{-1} \begin{bmatrix} O_{11} & 0 & O_{13} \\ O_{21} & -I & O_{23} \\ O_{31} & 0 & O_{33} \end{bmatrix} \begin{bmatrix} \overline{\Phi}_1 \\ \Phi_2 \\ \overline{\Phi}_3 \end{bmatrix}^{k+1} \tag{27}$$

(3) The iterative scheme

1. By substituting Eqs. (19) $\sim$ (21) into Eq. (18), initial values for the normal derivative of the velocity potentials on the water surface, $\partial\Phi_2^k/\partial\nu$, the velocity potentials on the pseudo wave-generator, Φ_1^k, as well as the velocity potentials on sea bed, Φ_3^k, can be obtained.

2. Tangential derivative of velocity potentials on water surface, $\partial\Phi_2^k/\partial s$, is then calculated using Eq. (22).

3. Surface elevations, (x^{k+1}, z^{k+1}), for the next time step can be obtained from Eqs. (24) and (25).

4. The velocity potentials on the free water surface for the next time step are given by Eq. (26).

5. At the next time step, t=(k+1)Δt, the coefficients of the matrix $[O]$ in Eq. (18) is recaculated, using profiles of the water surface obtained in procedure 3 and the new position of the pseudo wave-paddle.

6. Substituting the velocity potentials on water surface obtained by procedure 4, the horizontal velocity $U(t)$ of the pseudo wave paddle given by Eq. (2), and the boundary condition on the sea bed given by Eq. (8) into Eq. (27), the normal derivative of velocity potentials $\overline{\Phi}_2^{k+1}$ on water surface, the velocity potentials Φ_1^{k+1} on the pseudo wave paddle, and the velocity potentials Φ_3^{k+1} on the sea bed at the k+1 time step can be obtained.

7. Repeating the above procedures 2 through 6, the time history for the generation, propagation and deformation of waves can be simulated.

III. NUMERICAL RESULTS AND DISCUSSIONS

3.1 Time Histories of Wave Profiles

To verify the present numerical scheme, the case of periodical waves running against a vertical wall is first considered. All incident waves are assumed to have an unique amplitude $\zeta_0 = 0.05h$, where h is the constant water depth, but with various dimensionless angular frequencies $\sigma^2 h/g$=0.125~1.00. The pseudo wave-paddle is placed at a distance of 5 times the wave length away from the origin of the coordinates. For the cases of vertical wall, $\Delta t = T/160$; at the initial time, $\Delta s = L/32$ on the free water surface, but when the waves began to propagate, Δs changes along with the different time step, and is defined as a distance between two close nodes. For the cases of the inclined slope which varied from 1:0 to 1:1, $\Delta s = L/40$ and $\Delta t = T/400$.

Figure 2 shows the calculated time histories of the generation of periodical wave, propagating and running up against a vertical wall. Figure 3 shows the cases of a sloping beach with the slope varied from 1:0 to 1:1. Figure 4 is a comparison of standing waves with various frequencies $\sigma^2 h/g$=0.125~1.00 impinging against a vertical wall.

Figure 5 shows the profiles of a progressive wave without reflection from the vertical wall. Compared to the 3rd order Stokes wave derived by Skjelbreia (1959), good agreement is achieved.

Figure 6 shows the time histories of the wave profile at the time when the incident wave is reflected by the wall, and a clapotis is formed. The results are also consistent with the theoretical results given by Tadjbaksh (1960). From Fig. 4 we find that the characteristics of the finite amplitude wave are also strong toward various steepness of incident wave.

3.2 Stability of the Numerical Model

The conservative property of the present numerical scheme is cross-checked by the continuum equations for mass and energy through the following formula:

$$\left.\begin{aligned} M &= \int_{\Gamma_2} \zeta dx \\ E &= T_e + V \\ T_e &= \frac{1}{2}\int_{\Gamma} \Phi \overline{\Phi} ds \\ V &= \frac{1}{2} g \int_{\Gamma_2} \zeta^2 dx \end{aligned}\right\} \tag{28}$$

where M denotes the mass of fluid, E is the total energy, Γ_2 is the boundary of the free water surface, T_e and V are, respectively, the kinetic and potential energies.

Figure 7(a) shows the results for the case of a periodical wave. The mass increases after generation of a wave crest and decreases at the trough, thus total mass should be approximately null after each period of wave. However, for the cases of periodical waves in this study, the averaged water level will accumulate when the waves are generated. Besides, since the pseudo paddle moves back and forth continuously,

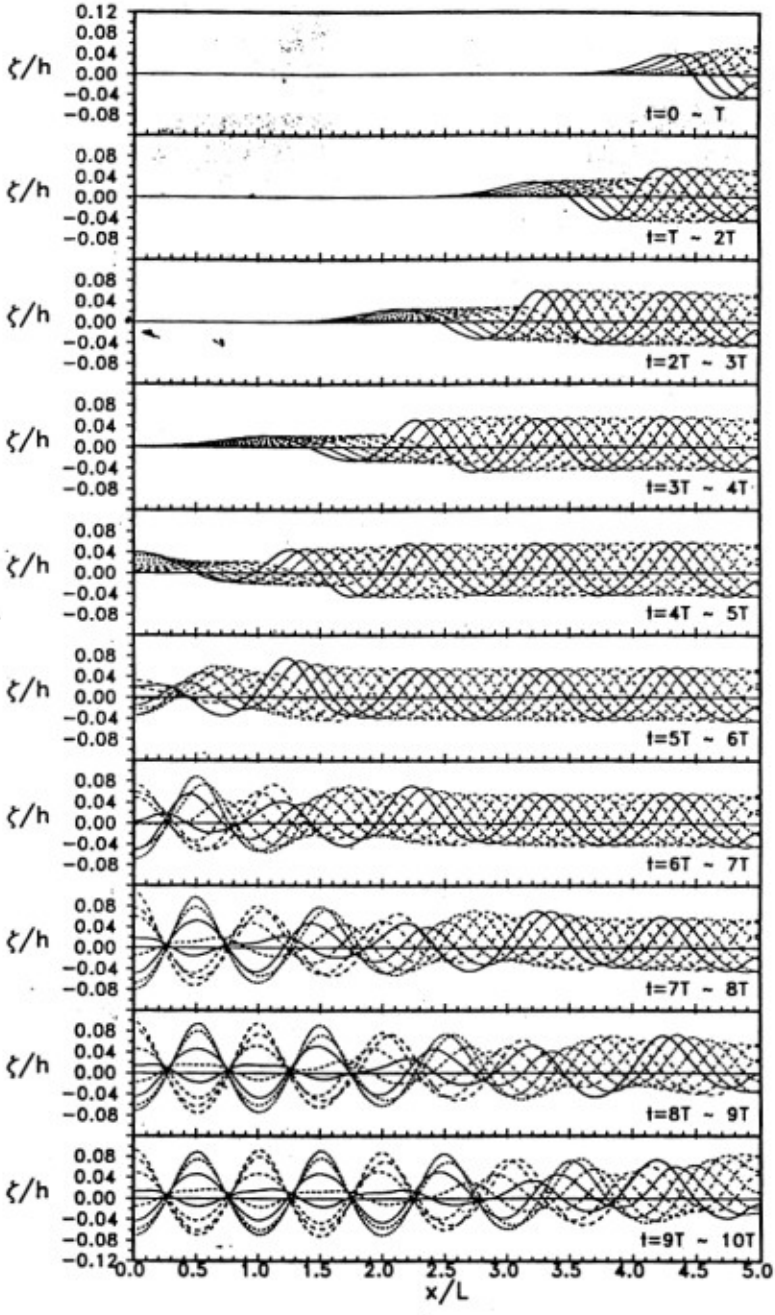

$\zeta_0/h = 0.05$, $\sigma^2 h/g = 0.50$, $\Delta t = T/160$, $\Delta s = L/32$

Fig. 2 Time histories of wave propagation and run-up against a vertical wall.

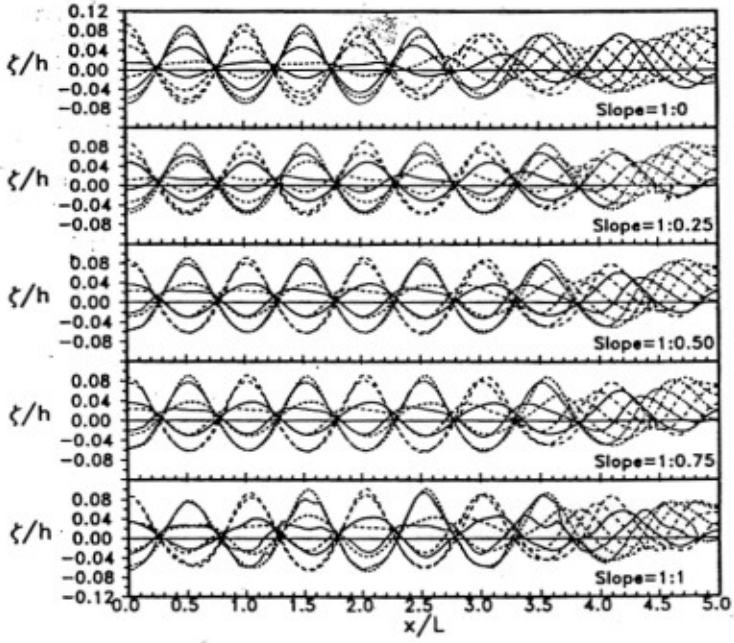

Fig. 3 Comparison of the profiles of standing wave on various slopes. ($\sigma^2 h/g = 0.50$)

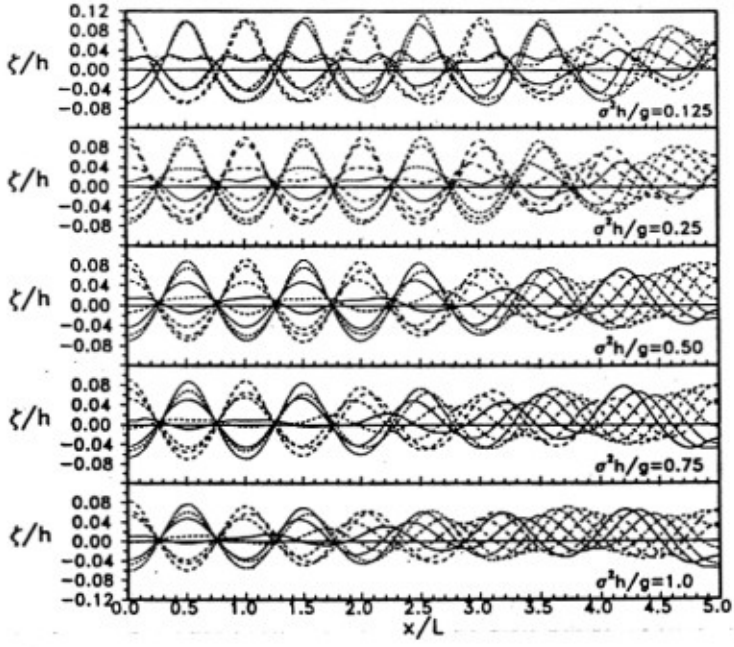

Fig. 4 Comparison of standing wave between various frequencies. (slope = 1 : 0)

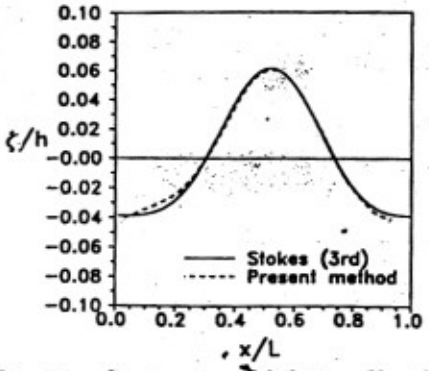

Fig. 5 Comparison of the profile of a progressive wave.

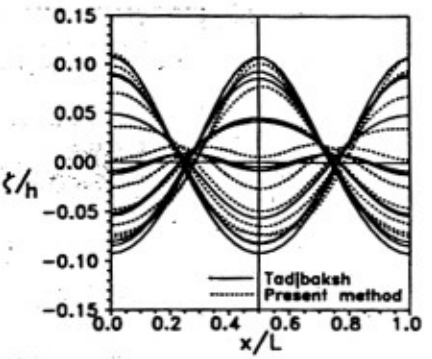

Fig. 6 Comparison of the profile of a clapotis.

according to the conservation of energy, the total energy is equal to the kinetic and potential energy that the pseudo paddle transmits, with a gradual increase of the total energy as a result. Due to the resonance of the clapotis, the oscillation of total energy becomes larger when the standing wave began to form gradually, the vertical dashed line in the figure shows the time when the wave reaches the wall. Also, the relation between kinetic and potential energy is shown in Fig. 7(b).

IV. DISTRIBUTIONS OF CURRENT VELOCITY

The current velocity at any inner point within the region can be derived from the velocity potential Φ and its normal derivative as $\partial\Phi/\partial\nu$ on the boundary. By Eq. (9), we obtain

$$\begin{aligned} u &= \frac{\partial\Phi(x,z;t)}{\partial x} \\ &= \frac{1}{2\pi}\sum_{j=1}^{n}\int_{\Gamma_j}\left\{\left(M_1\overline{\Phi}_j(\xi,\eta;t)+M_2\overline{\Phi}_{j+1}(\xi,\eta;t)\right)\left(\frac{x-\xi}{r^2}\right)\right. \\ &\quad -\left(M_1\Phi_j(\xi,\eta;t)+M_2\Phi_{j+1}(\xi,\eta;t)\right)\left[\nu_x\left(\frac{1}{r^2}-\frac{2(x-\xi)^2}{r^4}\right)\right. \\ &\quad \left.\left.-\nu_z\frac{(x-\xi)(z-\eta)}{r^4}\right]\right\}ds_j \end{aligned} \tag{29}$$

$$\begin{aligned} w &= \frac{\partial\Phi(x,z;t)}{\partial z} \\ &= \frac{1}{2\pi}\sum_{j=1}^{n}\int_{\Gamma_j}\left\{\left(M_1\overline{\Phi}_j(\xi,\eta;t)+M_2\overline{\Phi}_{j+1}(\xi,\eta;t)\right)\left(\frac{z-\eta}{r^2}\right)\right. \\ &\quad -\left(M_1\Phi_j(\xi,\eta;t)+M_2\Phi_{j+1}(\xi,\eta;t)\right)\left[\nu_z\left(\frac{1}{r^2}-\frac{2(z-\eta)^2}{r^4}\right)\right. \\ &\quad \left.\left.-\nu_x\frac{(x-\xi)(z-\eta)}{r^4}\right]\right\}ds_j \end{aligned} \tag{30}$$

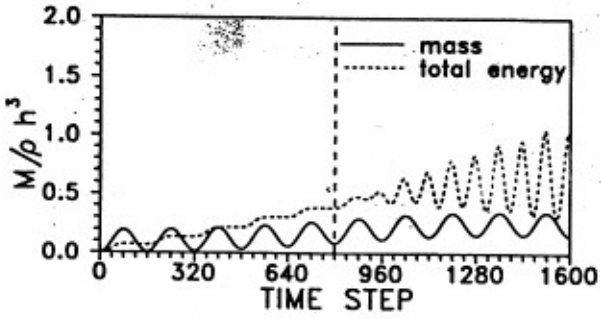

(a)

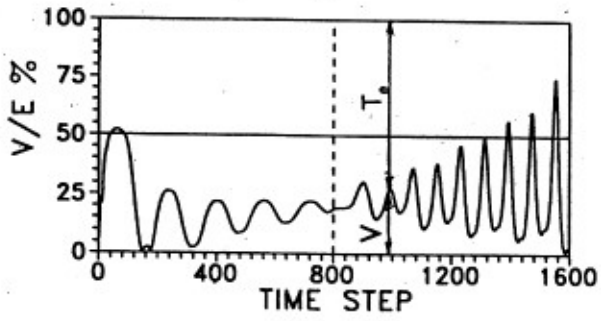

(b)

$\zeta_0/h = 0.05$, $\sigma^2 h/g = 0.25$, $\Delta s = L/32$, $\Delta t = T/160$

Fig. 7 Variation of mass and energy.

where ν_x and ν_z are the components of normal vector ν in the directions of x and z on the boundary.

Figures 8(a)~(h) show the distribution of current velocity for a progressive periodical wave with a time increment of 1/8 period of the wave. For progressive waves, the water surface displacement shows that each wave profile shifts without changing its shape. Since the wave profiles travel from the pseudo paddle to the wall, the distribution of the current velocity for each period of wave shifts from the right to the left gradually. Besides, from the enlarged figure shown in Figs. 9(a)~(h), it is found that each fixed point within the region has a velocity with the angle varying from 0 to 360 degree. This indicates that the movement of the fluid particles is circular as shown in Fig. 12(a). However, for finite waves, the path of each moving particle does not form as a closed circle. The wave profile is included at the top of the figure.

Furthermore, when clapotis is formed, the particle on each node shuttles only left and right, while the ones on the crest or trough move only up and down. The time histories for the distribution of current velocity are also shown in Figs. 10(a)~(h), as well as the enlarged figures in Figs. 11(a)~(h). Fig. 12(b) shows the movement of the fluid particles.

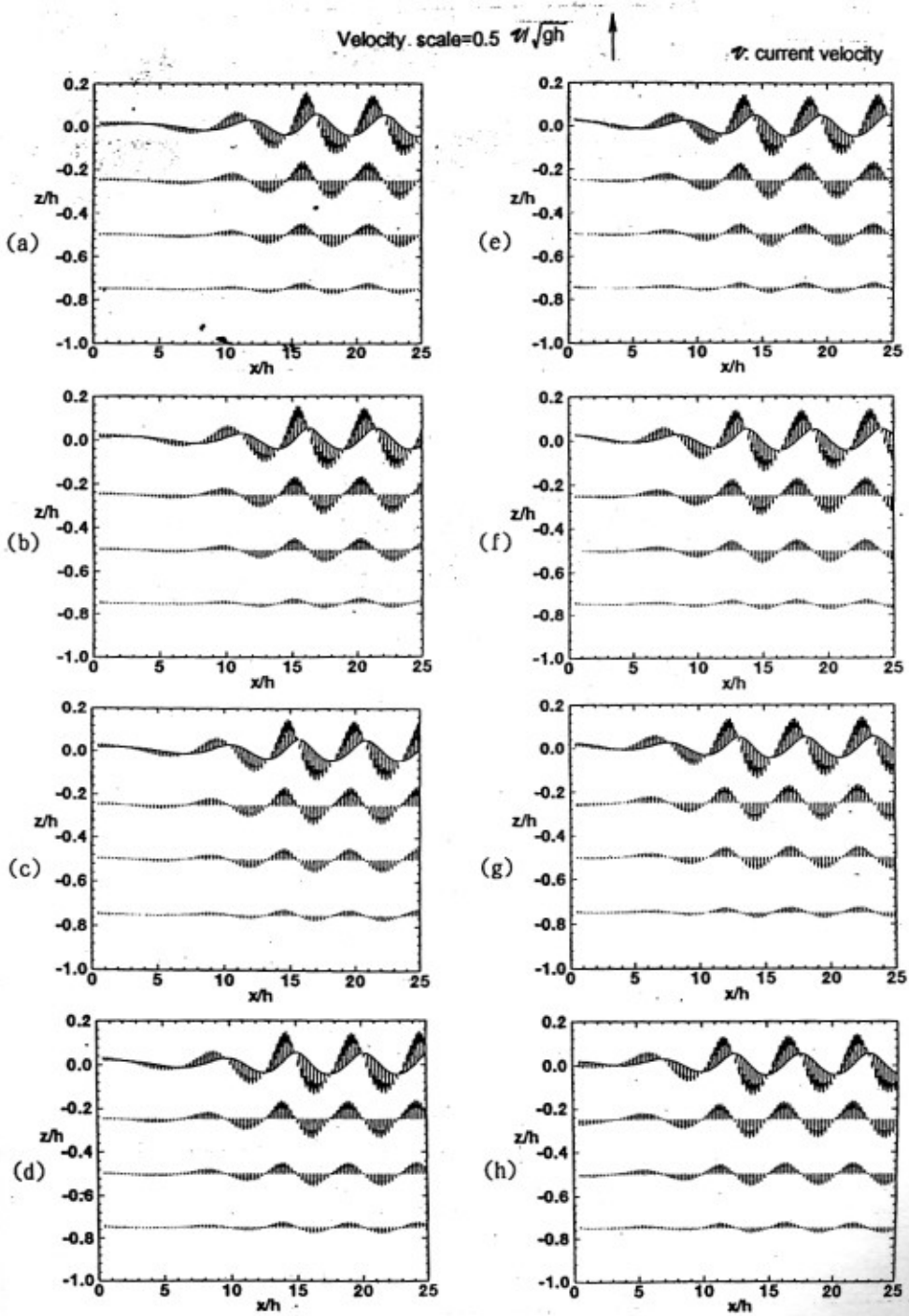

Fig. 8 Time history of the distribution of current velocity for progressive wave.

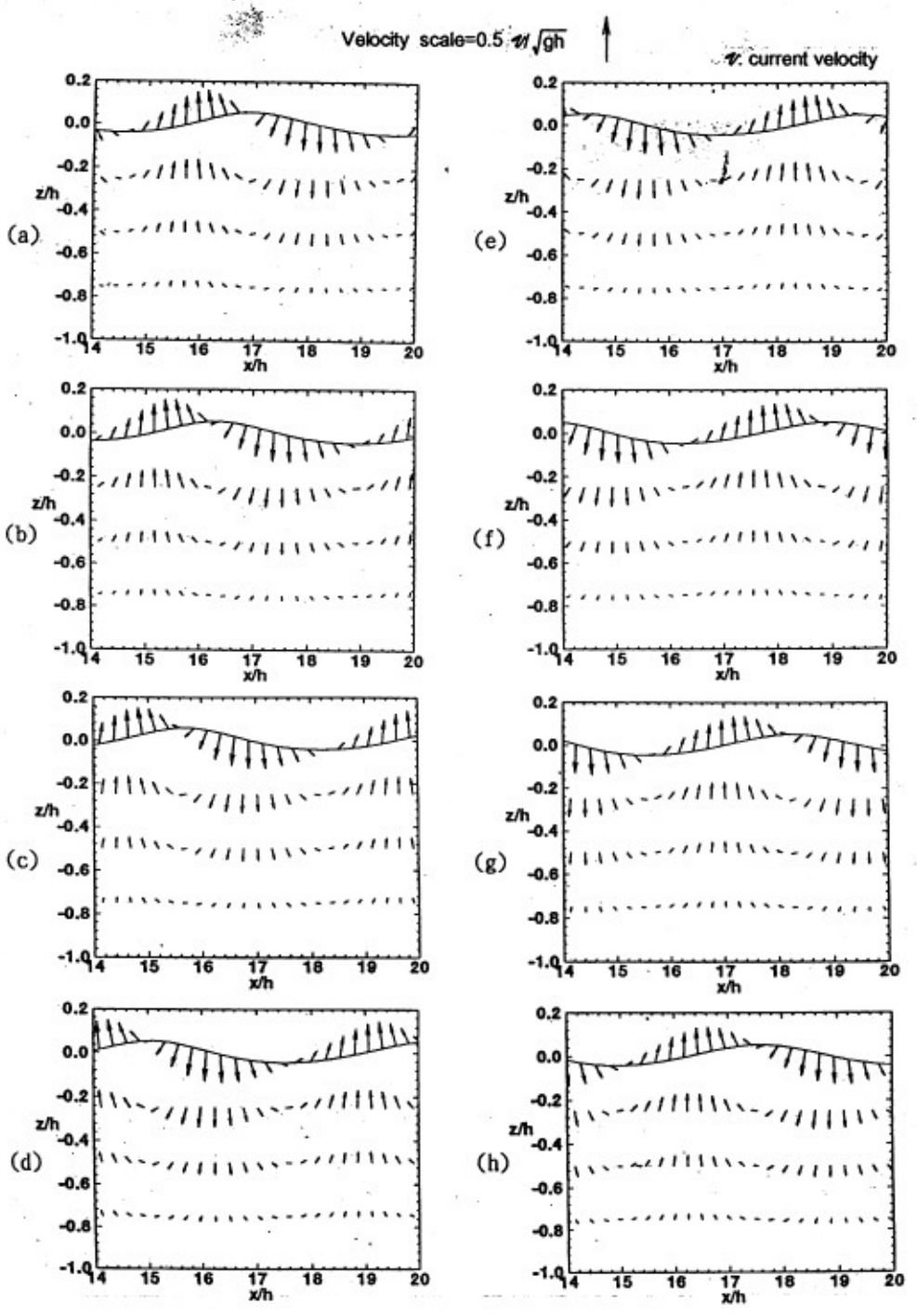

Fig. 9 Distribution of current velocity for one period of progressive wave.

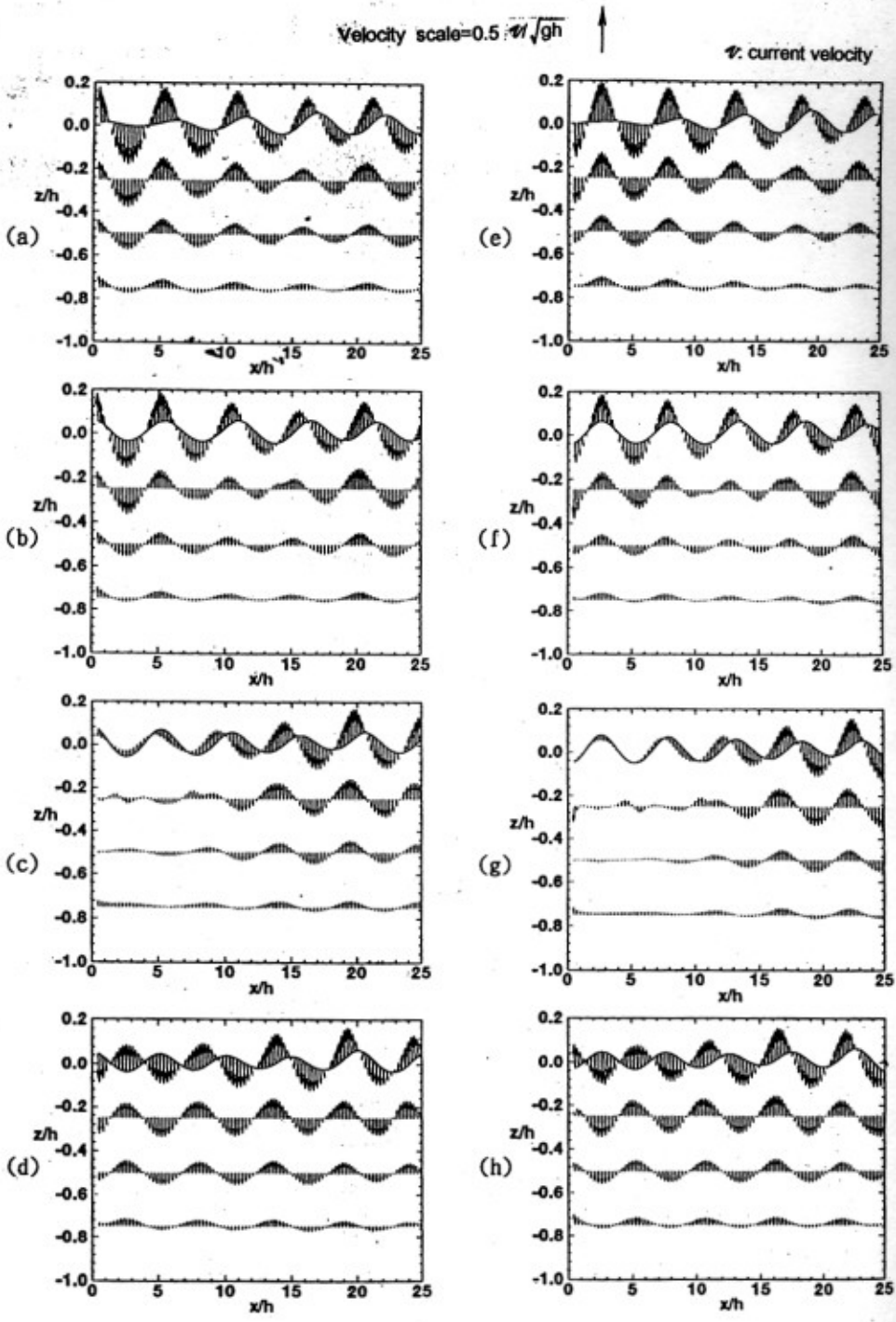

Fig. 10 Time history of the distribution of current velocity for standing wave.

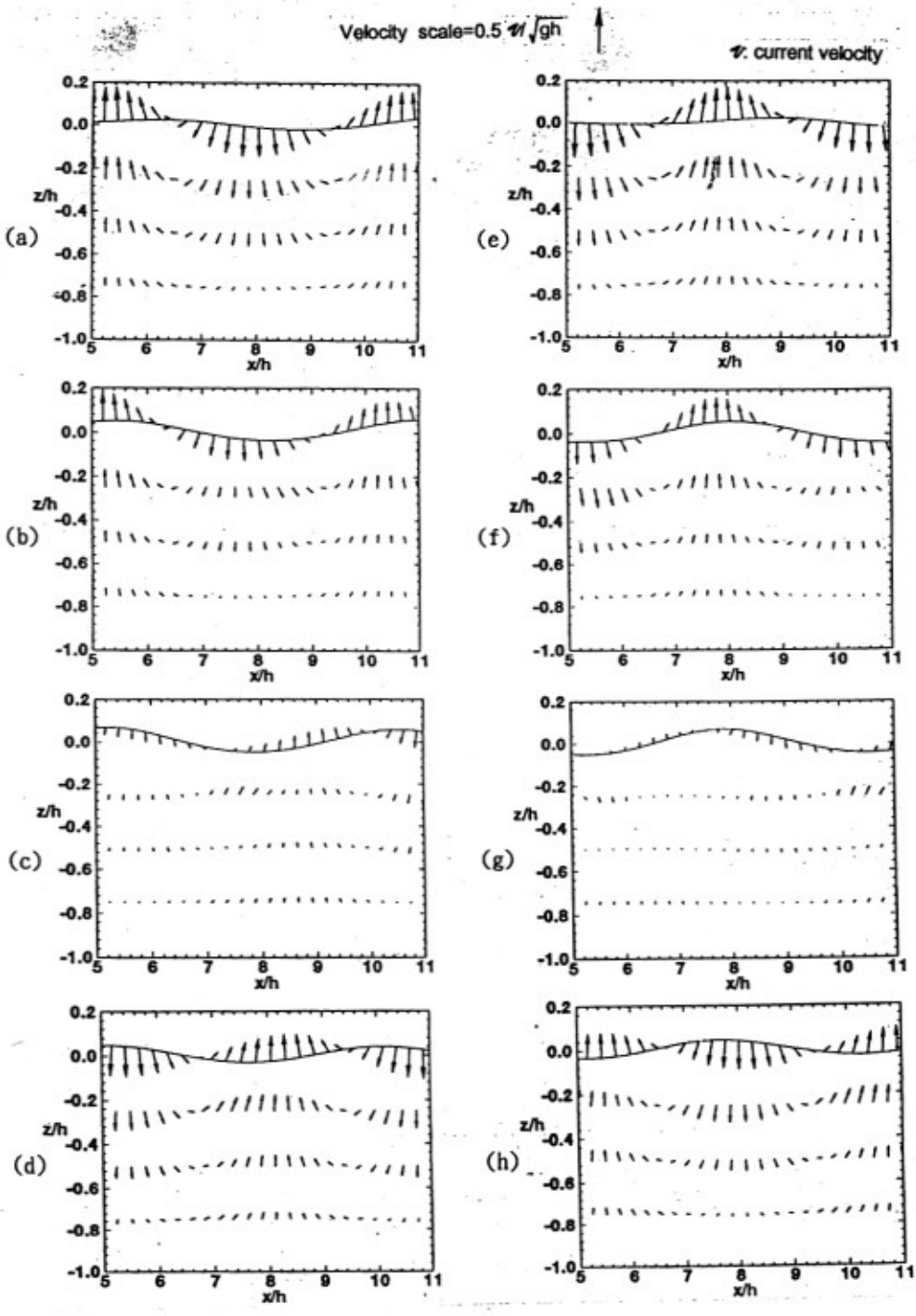

Fig. 11 Distribution of current velocity for one period of standing wave.

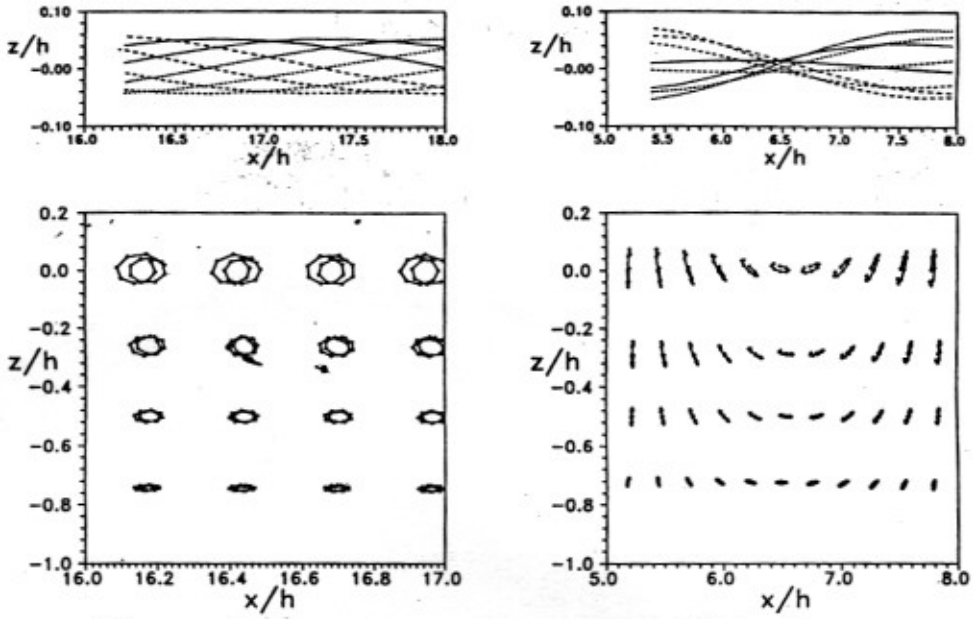

(a) progressive wave. (b) standing wave.

Fig. 12 The paths of the fluid particles.

V. CONCLUSIONS

In this article, an algorithm is derived to analyze the generation and propagation of two dimensional nonlinear periodic waves. It was found that the numerical instability of the present scheme appears for slopes greater than 1:1. In other cases, reasonable results for the generated waves as well as the current velocity were obtained.

ACKNOWLEDGEMENTS

This study was sponsored by the National Science Council of the Republic of China under the grant NSC-84-2611-E-0190-006. Advice and financial support of the council are gratefully acknowledged.

REFERENCES

Brorsen, M. and J. Larsen (1987): Source generation of nonlinear gravity waves with the boundary integral equation method, Coastal Eng., Vol. 10, No. 4, pp. 93–113.

Chou, C. R. (1983): The application of Boundary Element Method to Water Wave Mechanics. National Taiwan College of Marine Science and Technology, Harbor & Ocean Eng. Press, Keelung, R. O. C., 1983. (in Chinese)

Chou, C. R., R. S. Shih and H. M. Fang (1996): Deformation of solitary wave in coastal zones, Proc. of the 7th Japan-China Symp. on Boundary Element Method, Elsevier Press, pp. 171–180.

Faltinsen, O. (1978): A numerical nonlinear method of sloshing in tanks with two-dimensional flow, Jour. of Ship Res., Vol. 22, No. 3, pp. 193–202.

Isaacson, M., K. F. Cheung, E. Mansard and M. D. Miles (1994): Transient wave propagation in a laboratory flume, Jour. of Hydr. Res., Vol. 31, No. 5, pp. 665–680.

Madsen, O. S. (1970): Waves generated by a piston-type wavemaker, Proc. 12th Coastal Eng. Conf., pp. 589–607.

Nakayama, T. (1983): Boundary element analysis of nonlinear water wave problems, Int. Jour. for Numerical Method in Eng., Vol. 19, pp. 953–970.

Skjelbrea, L. (1959): Gravity waves, Stokes 3rd order approximation, Table of functions, The Eng. Foundation, Univ. of Cal. at Berkeley.

Tadjbaksh, L. D. and J. B. Keller (1960): Standing surface wave of finite amplitude, J. Fluid Mech., Vol. 8, pp. 442–451.

Wu, G. X. and R. E. Taylor (1994): Finite element analysis of two-dimensional non-linear transient water waves, Applied Ocean Res., Vol. 16, pp. 363–372.

(Received May 30, 1996; Revised Sep. 15, 1996)